AIP | Applied Physics Letters

Thermal conduction inhomogeneity of nanocrystalline diamond films by dual-side thermoreflectance

Elah Bozorg-Grayeli, Aditya Sood, Mehdi Asheghi, Vincent Gambin, Rajinder Sandhu et al.

Citation: Appl. Phys. Lett. **102**, 111907 (2013); doi: 10.1063/1.4796168
View online: http://dx.doi.org/10.1063/1.4796168
View Table of Contents: http://apl.aip.org/resource/1/APPLAB/v102/i11
Published by the American Institute of Physics.

Related Articles

Coupled vibrational modes in multiple-filled skutterudites and the effects on lattice thermal conductivity reduction
Appl. Phys. Lett. 102, 111905 (2013)

Nanowire-filled polymer composites with ultrahigh thermal conductivity
Appl. Phys. Lett. 102, 093117 (2013)

Thermal conductivity predictions of herringbone graphite nanofibers using molecular dynamics simulations
J. Chem. Phys. 138, 084708 (2013)

Cross-plane thermal properties of transition metal dichalcogenides
Appl. Phys. Lett. 102, 081604 (2013)

Thermoelectric properties of p-type (Bi2Te3)x(Sb2Te3)1−x single crystals doped with 3wt. % Te
J. Appl. Phys. 113, 073709 (2013)

Additional information on Appl. Phys. Lett.

Journal Homepage: http://apl.aip.org/
Journal Information: http://apl.aip.org/about/about_the_journal
Top downloads: http://apl.aip.org/features/most_downloaded
Information for Authors: http://apl.aip.org/authors

ADVERTISEMENT

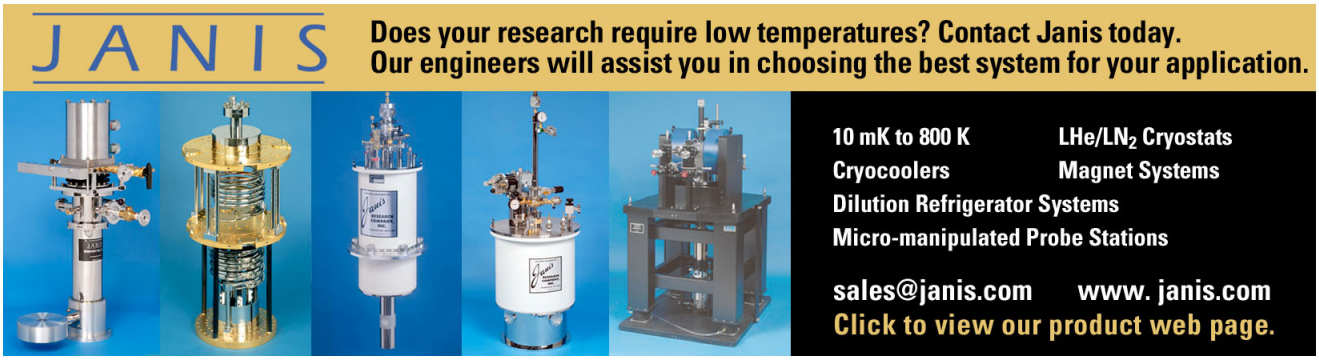

Thermal conduction inhomogeneity of nanocrystalline diamond films by dual-side thermoreflectance

Elah Bozorg-Grayeli,[1,a)] Aditya Sood,[1,2] Mehdi Asheghi,[1] Vincent Gambin,[3] Rajinder Sandhu,[3] Tatyana I. Feygelson,[4] Bradford B. Pate,[5] Karl Hobart,[5] and Kenneth E. Goodson[1]

[1]*Department of Mechanical Engineering, Stanford University, Stanford, California 94305, USA*
[2]*Department of Materials Science and Engineering, Stanford University, Stanford, California 94305, USA*
[3]*Northrop Grumman Corporation, San Diego, California 92127, USA*
[4]*Science Applications International Corporation, McLean, Virginia 22102, USA*
[5]*Naval Research Laboratory, Washington, DC 20375, USA*

(Received 10 December 2012; accepted 8 March 2013; published online 20 March 2013)

Thin diamond films of thickness near 1 μm can have highly nonuniform thermal conductivities owing to spatially varying disorder associated with nucleation and grain coalescence. Here, we examine the nonuniformity for nanocrystalline chemical vapor deposited diamond films of thickness 0.5, 1.0, and 5.6 μm using picosecond thermoreflectance from both the top and bottom diamond surfaces, enabled by etching a window in the silicon substrate. The extracted local thermal conductivities vary from less than 100 $\mathrm{W\,m^{-1}\,K^{-1}}$ to more than 1300 $\mathrm{W\,m^{-1}\,K^{-1}}$ and suggest that the most defective material is confined to within 1 μm of the growth surface. © *2013 American Institute of Physics*. [http://dx.doi.org/10.1063/1.4796168]

Diamond is a promising potential successor to Si and SiC as a thermal spreader for high electron mobility transistors based on GaN.[1–5] Based on much research over the past several decades, chemical vapor deposition of diamond has become well established[6–11] and has led to routine deposition of polycrystalline and nanocrystalline diamond thin films. A remaining challenge is to integrate diamond materials into high power device structures in order to take advantage of the high thermal conductivity. Diamond thin film deposition requires a seed layer to nucleate film growth on a foreign substrate. In this work, the seeds are nanodiamonds (typically 5–10 nm diamond particles) spread at roughly 10^{12} seeds/cm^2 on the silicon substrate before growth. During the initial stage of deposition, the seed layer coalesces into a continuous film. The deposited film is fully coalesced at 300 nm thickness. Beyond the initial coalescence layer, there is predominantly columnar growth normal to the silicon-diamond interface.[11] Unfortunately, if the thermal resistance due to the film coalescence layer is sufficiently large, diamond thin films with a coalescence region between the high conductivity diamond bulk and the heat source may not offer a thermal advantage over Si or SiC.[12,13]

Theoretically, isotopically enriched single-crystal diamond might eventually offer thermal conductivities up to 5000 $\mathrm{W\,m^{-1}\,K^{-1}}$ at room temperature, and experiments on isotopically enriched diamond have shown thermal conductivity as high as 3300 $\mathrm{W\,m^{-1}\,K^{-1}}$.[14–16] For polycrystalline diamond films less than several hundred micrometers thick, the cross-plane thermal conductivity is typically much lower, near 1000 $\mathrm{W\,m^{-1}\,K^{-1}}$ at room temperature.[17,18] Several factors impede the mean free path (MFP) of phonons in these polycrystalline diamond films and reduce the thermal conductivity. These include impurity scattering, grain boundary scattering, and interface scattering.[17–20] At the initial stage of diamond thin film deposition, these scattering mechanisms are very strong and significantly reduce the thermal conductivity.[20] This defective material, which we refer to here as the "coalescence region," is usually buried underneath several μm of columnar diamond grains, making the thermal properties difficult to extract. Since the coalescence region strongly affects the diamond thermal performance, it is critical to develop a technique which can extract the thermal properties of both the coalescence and columnar diamond regions.

Here, we perform picosecond time-domain thermoreflectance (TDTR) measurements on the top and bottom surfaces of suspended nanocrystalline diamond films from 0.5 μm to 5.6 μm in thickness. By probing both sides of the suspended film, we capture the cross-plane thermal conductivity of both the coalescence region (k_C) and the high-quality columnar grain (k_{HQ}) regions. To simplify interpretation, we develop a two-layer heat diffusion model within the diamond film, which approximately separates the coalescence and bulk regions. While this approach is at best an approximation to the continuously varying phonon scattering rates in the direction normal to the film, a two-region model is a reasonable first approximation and is consistent with the level of detail that can be obtained using the TDTR approach.[21] We estimate the thickness of the low conductivity coalescence layer and compare the thermal resistances of the coalescence versus high-quality regions. This analysis demonstrates that the coalescence region can be a substantial contributor to thermal resistance in a diamond thin film.

Picosecond TDTR uses the temperature-dependent optical properties of a thin metal transducer as a thermometer for a heated thin film stack.[22,23] Our TDTR system uses a passively modelocked Nd:YVO_4 laser with 9.2 ps pulsewidth, 10 μm pump beam diameter, 5 μm probe beam diameter, and 82 MHz repetition rate.[24,25] We then use a radially symmetric model of heat diffusion through a multilayer stack to fit

[a)]Electronic mail: ebozorgg@stanford.edu

 © 2013 American Institute of Physics

for the transducer-film thermal boundary resistance (TBR), the intrinsic thermal conductivity of the film, and the film-substrate TBR.[26,27]

The heat capacitance of the diamond coalescence region is small compared to the total heat capacitance of the diamond film, and the coalescence region is several μm from the transducer film. As a result, the properties of the additional coalescence layer are very difficult to extract separately from the diamond-silicon thermal boundary resistance.[13] In order to separate the two properties, we require direct contact between the transducer layer and the coalescence layer. This involves removal of the silicon substrate to allow deposition of a metal transducer directly on the seeded surface of the coalescence region. To accomplish this, we deposited three nanocrystalline diamond films on silicon substrates of thicknesses 0.5 μm, 1.0 μm, and 5.6 μm. The silicon substrates were selectively etched to produce a suspended diamond thin film of roughly 5 μm in diameter. A 50 nm Al transducer layer was deposited on each side of the suspended diamond film (Fig. 1).

When the characteristic thermal decay time of the film of interest is less than the measurement time scale, and the film is effectively insulated during the measurement time scale, the temperature decay of the transducer film depends primarily on the heat capacity and total thermal resistance of the film of interest. For the case of the 0.5 μm film, we obtain only an effective thermal resistance for the diamond film of $20 \pm 2.0\ \mathrm{m^2\,K\,GW^{-1}}$, which can be expressed as

$$R_{eff} = R_{Al-diam} + \frac{d_{diam}}{k_C}, \tag{1}$$

where R_{eff} is the effective resistance of the diamond film, $R_{Al\text{-}diam}$ is the aluminum-diamond TBR, and d_{diam} is the thickness of the diamond film. We convert this to an effective thermal conductivity of the diamond layer by dividing the film thickness by the resistance. This gives a value of $k_{eff,C}$ of approximately $25\ \mathrm{W\,m^{-1}\,K^{-1}}$. Using the previously reported diamond heat capacity[28] $\sim 2.15 \times 10^6\ \mathrm{J\,m^{-3}\,K^{-1}}$, this translates to a total thermal diffusivity of $\sim 1.16 \times 10^{-5}\ \mathrm{m^2\,s^{-1}}$. The characteristic thermal decay time of the diamond, determined via

$$\tau_{diam} = \frac{d_{diam}^2}{\alpha_{eff}}, \tag{2}$$

where α_{eff} is the effective thermal diffusivity, is $\sim$22 ns. The characteristic timescale of the heating event, however, is given by the inverse of the 5 MHz pump modulation frequency. This translates to a heating timescale of 200 ns, significantly greater than τ_{diam}. Therefore, although measurements on this sample are insensitive to the difference between intrinsic and thermal boundary resistance, we can uniquely extract the diamond heat capacity. The fitted heat capacity, $1.98 \times 10^6\ \mathrm{J\,m^{-3}\,K^{-1}}$, is similar to previous literature results.[28]

In order to separate out k_C and $R_{Al\text{-}diam}$ from the effective thermal resistance, we use the 1.0 μm thick diamond film. While τ_{diam} for this film ($\sim$56 ns) is still less than the timescale of the measurement, we have sufficient sensitivity to separate the transducer-film TBR from the intrinsic film thermal conductivity. Modeling the system as 50 nm Al on 1.0 μm diamond, we extract a TBR of $13.5 \pm 1.0\ \mathrm{m^2\,K\,GW^{-1}}$ between the Al transducer and the diamond coalescence layer. Further, we find a cross-plane thermal conductivity of $80 \pm 10\ \mathrm{W\,m^{-1}\,K^{-1}}$ for the diamond coalescence layer. By applying these results to Eq. (1) and setting d_{diam} to 0.5 μm, we obtain a total thermal resistance that agrees with the value measured from the 0.5 μm diamond sample. Comparing the results with the model of local diamond thermal conductivity developed by Touzelbaev and Goodson indicates an average coalescence layer grain size of 100–200 nm.[20]

We determine the thickness of the thermally resistive coalescence layer using the 5.6 μm diamond film. Picosecond TDTR measurements on the top side of the diamond reveal an Al-diamond thermal boundary resistance of $10.7 \pm 1.0\ \mathrm{m^2\,K\,GW^{-1}}$, smaller than for the Al-coalescence layer interface. Since the thermal boundary resistance is highly dependent on surface cleanliness, this difference may be due to impurities left behind by the etching process on the bottom diamond film surface. Assuming the heat capacity measured from the 0.5 μm sample, and using a one-layer model of 50 nm Al on 5.6 μm diamond, we find a cross-plane thermal conductivity of $1350 \pm 200\ \mathrm{W\,m^{-1}\,K^{-1}}$ for the high-quality diamond (Fig. 2). It is worth noting that the result of

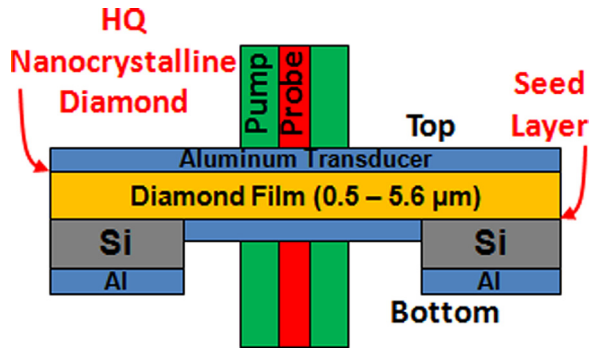

FIG. 1. Cross-sectional diagram of the suspended diamond film sample showing the Al transducer interface with the seeding/coalescence layer and with the HQ nanocrystalline diamond surface. Note that silicon has been etched to give access to the seeded surface of the diamond film where film coalescence occurs. The Al transducer layer is 50 nm thick, and the etched hole in silicon is $\sim$5 mm in diameter. The red and green areas indicate the probe and pump beams, respectively.

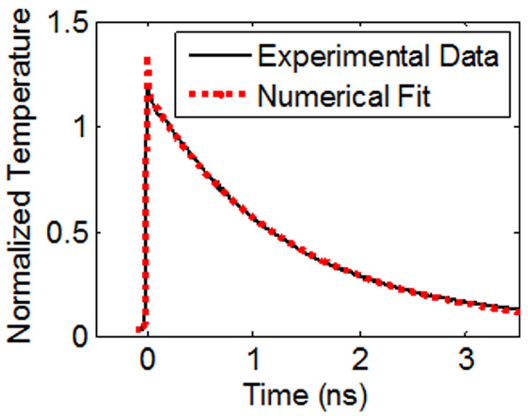

FIG. 2. Picosecond TDTR data (solid line) and numerical fit (dotted line) for the top side measurement of the 5.6 μm diamond film. The fit corresponds to an Al-diamond thermal boundary resistance of $10.7 \pm 1.0\ \mathrm{m^2\,K\,GW^{-1}}$ and a diamond thermal conductivity of $1350 \pm 200\ \mathrm{W\,m^{-1}\,K^{-1}}$.

the numerical fit for this sample remains the same even assuming a diamond thickness as low as 2.5 μm. This implies the top side measurement may be insensitive to the coalescence layer properties.

To confirm this hypothesis, we performed TDTR on the bottom of the same sample. Figure 3 demonstrates the difference in the thermoreflectance curves for the two measurements, showing a significantly slower thermal decay through the coalescence-layer. Using the coalescence layer diamond data from the 5.6 μm thick film, we created a two-layer model of heat conduction through the suspended film. This model assumes 50 nm of Al on a diamond coalescence layer with unknown thickness, d_C, on a high-quality diamond layer of thickness $d_{HQ} = 5.6\ \mu\text{m}\text{-}d_C$. Assuming $k_C = 80\ \text{W m}^{-1}\text{K}^{-1}$ and $k_{HQ} = 1350\ \text{W m}^{-1}\text{K}^{-1}$, we fit for the coalescence layer thickness and find $d_C = 0.76 \pm 0.1\ \mu$m. The thickness of the high quality diamond layer, therefore, is $\sim$4.84 μm, thick enough to render the top side measurements insensitive to the thermal properties of the coalescence layer diamond. This validates the one-layer assumption used for the top side measurement of the 5.6 μm sample.

The thickness prediction for the coalescence layer is more subtle than the two-layer model implies. Although the diamond film consists of columnar grains on a thin coalescence layer, there is no sharp transition between the two. Rather, the average grain size in the film increases smoothly as a function of distance from the substrate surface. What the two-layer model determines is an estimated thickness based on the thermal conductivity measured in the thinner samples. If we assume a higher thermal conductivity, the fitted coalescence layer thickness increases proportionally. A more robust comparison would involve the thermal resistances of the two layers. Although the fitted thickness of the coalescence layer depends proportionally on the assumed thermal conductivity, the fitted thermal resistance of the layer remains the same regardless of assumed thermal conductivity.

The thermal properties of the diamond film coalescence layer have a dominant influence on the total thermal resistance of the film. Using the coalescence layer thickness and thermal conductivity we estimated using the two-layer model, we find, for a 5.6 μm diamond film, that the coalescence layer thermal resistance ($R_C = d_C/k_C$) is $\sim 9.5 \pm 1.4\ \text{m}^2\,\text{K GW}^{-1}$. This is significantly larger than the thermal resistance of the rest of the diamond film ($\sim 3.6 \pm 0.6\ \text{m}^2\,\text{K GW}^{-1}$ assuming a 0.76 μm coalescence layer). In fact, the coalescence layer has a thermal resistance equivalent to $\sim$12.8 μm of high quality diamond.

Understanding the contribution of ballistic phonons to conduction in such high thermal conductivity materials is essential. First, when the spatial extent of the heated region is smaller than the mean free paths of a significant fraction of the phonons responsible for heat conduction, the resulting temperature field can be influenced by partially ballistic (rather than diffusive) transport.[29–31] Second, when the thermal penetration depth is comparable to the mean free paths of a substantial number of phonons, the interpretation of TDTR data becomes challenging, as our analysis assumes Fourier like diffusive behavior within each layer of the sample stack. In order to quantify the contribution of ballistic phonons in our polycrystalline diamond films, we employ a Debye thermal conductivity model with multiple sources of phonon scattering arising out of lattice anharmonicity and defects.[32] In this calculation, Umklapp and normal processes are described using parameters taken from Wei *et al.*[16] Point defects (vacancy concentration $= 3 \times 10^{18}\ \text{cm}^{-3}$), extended defects (diameter = 1.5 nm, concentration $= 5 \times 10^{16}\ \text{cm}^{-3}$), and dislocations (density $= 10^{12}\ \text{cm}^{-2}$) are described using values reported in Graebner *et al.* for diamond samples of comparable conductivity.[17] Diffuse phonon scattering at grain boundaries (average grain size = 1 μm) and film surfaces (film thickness = 5.6 μm) are also taken into account in calculating the total scattering rate. Figure 4 plots the accumulation of thermal conductivity as a function of phonon mean free path, showing that about 90% of the contribution to heat conduction is by phonons with a mean free path smaller than about 350 nm. This length scale is more than an order of magnitude smaller than the thermal penetration depth (2.5 μm) and film thickness, supporting our analysis of the TDTR data based on a diffusive model. Furthermore,

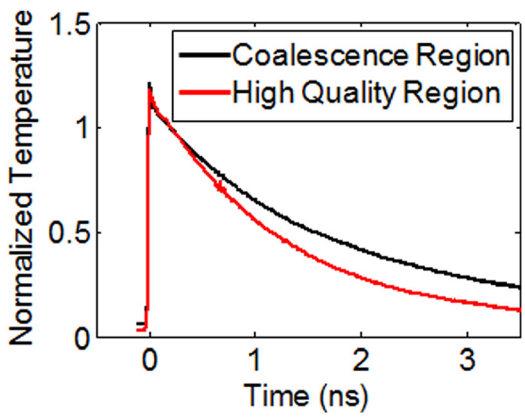

FIG. 3. Comparison of picosecond TDTR curves from the coalescence and high quality layers of the 5.6 μm diamond sample. The larger, higher quality diamond grains on the top surface result in a higher thermal conductivity than for the bottom. This is evidenced by the faster thermal decay shown for the high quality layer.

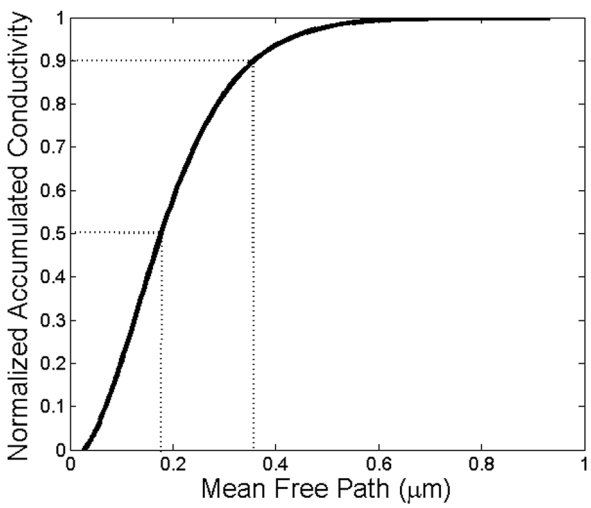

FIG. 4. Thermal conductivity (cross-plane) accumulation with phonon mean free path for a thin diamond film, calculated using the model from Graebner *et al.*,[32] with lattice and defect scattering parameters as specified in the text. The dotted lines indicate that phonons with mean free paths smaller than 350 nm contribute to about 90% of the heat conduction.

since the laser spot size (10 μm) is much larger than the maximum mean free path, the effect of phonons conducting out of the heater region in a ballistic manner is not significant.

This work extracts the thermal conductivity nonuniformity in nanocrystalline diamond films of thickness near 5 μm using dual-sided picosecond TDTR measurements. This technique extracted the thermal conductivity of the coalescence layer, the high quality diamond layer, and the heat capacity of the suspended films. From these results, we estimate the coalescence layer thickness and calculate the thermal resistance contributions of both regions of the diamond film. The additional coalescence layer thermal resistance is significant. Further research into nanocrystalline diamond nucleation and growth may improve the coalescence layer thermal properties, reducing the total thermal resistance and enhancing the thermal performance of integrated nanocrystalline diamond thermal spreaders for high-power transistor applications.

This research was made with private and Government support and was awarded by Northrop Grumman (agreement # 7600011363, titled: Thermal Reflectance Material Characterization Supporting the NEXT Program Phase I&II), DARPA (agreement # FE 01 19 12, titled: GaN-on-Diamond Thermal Measurements and agreement # RFMD-12-C-0002, titled: Thermal Characterization of GaN-on-Diamond Materials and PA Devices), and the AFOSR (agreement # FA9550-12-1-0195, titled: Multicarrier and Low-Dimensional Thermal Conduction at Interfaces for High Power Electronic Devices).

[1]G. H. Jessen, J. K. Gillespie, G. D. Via, A. Crespo, D. Langley, J. Wasserbauer, F. Faili, D. Francis, D. Babic, F. Ejeckam, S. Guo, and I. Eliashevich, *AlGaN/GaN HEMT on Diamond Technology Demonstration* (CSIC, 2006), pp. 271–274.
[2]J. G. Felbinger, M. V. S. Chandra, S. Yunju, L. F. Eastman, J. Wasserbauer, F. Faili, D. Babic, D. Francis, and F. Ejeckam, IEEE Electron Device Lett. **28**, 948–950 (2007).
[3]Q. Diduck, J. Felbinger, L. F. Eastman, D. Francis, J. Wasserbauer, F. Faili, D. I. Babic, and F. Ejeckam, Electron. Lett. **45**, 758–759 (2009).
[4]M. J. Tadjer, T. J. Anderson, K. D. Hobart, T. I. Feygelson, J. D. Caldwell, C. R. Eddy, F. J. Kub, J. E. Butler, B. Pate, and J. Melngailis, IEEE Electron Device Lett. **33**, 23–25 (2012).
[5]C. Jungwan, L. Zijian, E. Bozorg-Grayeli, T. Kodama, D. Francis, F. Ejeckam, F. Faili, M. Asheghi, and K. E. Goodson, "Thermal characterization of GaN-on-diamond substrates for HEMT applications," in *ITHERM 2012*, San Diego, CA, pp. 435–439.
[6]J. C. Angus, H. A. Will, and W. S. Stanko, J. Appl. Phys. **39**, 2915–2922 (1968).
[7]B. V. Spitsyn, L. L. Bouilov, and B. V. Derjaguin, J. Cryst. Growth **52**(Part 1), 219–226 (1981).
[8]M. Kamo, Y. Sato, S. Matsumoto, and N. Setaka, J. Cryst. Growth **62**, 642–644 (1983).
[9]Y. Hirose and Y. Terasawa, Jpn. J. Appl. Phys., Part 2 **25**, L519–L521 (1986).
[10]M. Kamo, H. Yurimoto, and Y. Sato, Appl. Surf. Sci. **33–34**, 553–560 (1988).
[11]J. Philip, P. Hess, T. Feygelson, J. E. Butler, S. Chattopadhyay, K. H. Chen, and L. C. Chen, J. Appl. Phys. **93**, 2164–2171 (2003).
[12]A. Aminfar, E. Bozorg Grayeli, M. Asheghi, and K. E. Goodson, "Analysis of HEMT multilayered structures using a 2D finite volume model," in *ITHERM 2012*, San Diego, CA, pp. 224–234.
[13]E. Bozorg-Grayeli, L. Zijian, V. Gambin, M. Asheghi, and K. E. Goodson, "Thermal conductivity, anisotropy, and interface resistances of diamond on poly-AlN," in *ITHERM 2012*, San Diego, CA, pp. 1059–1064.
[14]G. A. Slack, J. Appl. Phys. **35**, 3460–3466 (1964).
[15]T. R. Anthony, W. F. Banholzer, J. F. Fleischer, L. Wei, P. K. Kuo, R. L. Thomas, and R. W. Pryor, Phys. Rev. B **42**, 1104–1111 (1990).
[16]L. Wei, P. K. Kuo, R. L. Thomas, T. R. Anthony, and W. F. Banholzer, Phys. Rev. Lett. **70**, 3764–3767 (1993).
[17]J. E. Graebner, S. Jin, G. W. Kammlott, J. A. Herb, and C. F. Gardinier, Nature **359**, 401–403 (1992).
[18]D. T. Morelli, C. P. Beetz, and T. A. Perry, J. Appl. Phys. **64**, 3063–3066 (1988).
[19]K. E. Goodson, O. W. Käding, M. Rösler, and R. Zachai, J. Appl. Phys. **77**, 1385–1392 (1995).
[20]M. N. Touzelbaev and K. E. Goodson, J. Thermophys. Heat Transfer **11**, 506–512 (1997).
[21]K. E. Goodson, J. Heat Transfer **118**, 279–286 (1996).
[22]K. Ujihara, J. Appl. Phys. **43**, 2376–2383 (1972).
[23]C. A. Paddock and G. L. Eesley, J. Appl. Phys. **60**, 285–290 (1986).
[24]M. A. Panzer, M. Shandalov, J. A. Rowlette, Y. Oshima, C. Yi Wei, P. C. McIntyre, and K. E. Goodson, IEEE Electron Device Lett. **30**, 1269–1271 (2009).
[25]J. P. Reifenberg, K.-W. Chang, M. A. Panzer, S. Kim, J. A. Rowlette, M. Asheghi, H.-S. P. Wong, and K. E. Goodson, IEEE Electron Device Lett. **31**, 56–58 (2010).
[26]A. Feldman, High Temp. - High Press. **31**, 293–298 (1999).
[27]D. G. Cahill, Rev. Sci, Instrum. **75**, 5119–5122 (2004).
[28]A. C. Victor, J. Chem. Phys. **36**, 1903–1911 (1962).
[29]P. G. Sverdrup, S. Sinha, M. Asheghi, S. Uma, and K. E. Goodon, Appl. Phys. Lett. **78**, 3331–3333 (2001).
[30]A. J. Minnich, J. A. Johnson, A. J. Schmidt, K. Esfarjani, M. S. Dresselhaus, K. A. Nelson, and G. Chen, Phys. Rev. Lett. **107**, 095901 (2011).
[31]M. E. Siemens, Q. Li, R. Yang, K. A. Nelson, E. H. Anderson, M. M. Murnane, and H. C. Kapteyn, Nature Mater. **9**, 26–30 (2010).
[32]J. E. Graebner, M. E. Reiss, L. Seibles, T. M. Hartnett, R. P. Miller, and C. J. Robinson, Phys. Rev. B **50**, 3702–3713 (1994).